DYSTONIA

TYPE Original Research
PUBLISHED 12 February 2025
DOI 10.3389/dyst.2025.13874

OPEN ACCESS

EDITED BY
Linda Hyoungsun Kim,
Texas Children's Hospital, United States

*CORRESPONDENCE
D. E. Vaillancourt,
vcourt@ufl.edu

RECEIVED 01 October 2024
ACCEPTED 23 January 2025
PUBLISHED 12 February 2025

CITATION
Adury RZ, Wilkes BJ, Girdhar P, Li Y and Vaillancourt DE (2025) Altered functional brain connectivity in Dyt1 knock-in mouse models. *Dystonia* 4:13874.
doi: 10.3389/dyst.2025.13874

Altered functional brain connectivity in Dyt1 knock-in mouse models

R. Z. Adury[1], B. J. Wilkes[1], P. Girdhar[2], Y. Li[2] and D. E. Vaillancourt[1,2,3]*

[1]Department of Applied Physiology and Kinesiology, University of Florida, Gainesville, FL, United States, [2]Department of Neurology, University of Florida, Gainesville, FL, United States, [3]Department of Biomedical Engineering, University of Florida, Gainesville, FL, United States

DYT1 dystonia is an early onset, generalized form of isolated dystonia characterized by sustained involuntary muscle co-contraction, leading to abnormal movements and postures. It is the most common hereditary form of primary dystonia, caused by a trinucleotide GAG deletion in the DYT1 gene, which encodes the TorsinA protein. Recent studies conceptualized dystonia as a functional network disorder involving basal ganglia, thalamus, cortex and cerebellum. However, how TorsinA dysfunction in specific cell types affects network connectivity and dystonia-related pathophysiology remains unclear. In this study, we aimed to elucidate the impact of the GAG TorsinA mutation present globally and when restricted to the cortical and hippocampal neurons. To accomplish this, we generated two distinct Dyt1 mouse models, one with Dyt1 dGAG knock-in throughout the body (dGAG) and another with a cerebral cortex-specific Dyt1 dGAG knock-in using Emx1 promoter (EMX). In both models, we performed *in vivo* neuroimaging at ultra-high field (11.1T). We employed functional magnetic resonance imaging (fMRI) to assess resting-state and sensory-evoked brain connectivity and activation, along with diffusion MRI (dMRI) to evaluate microstructural changes. We hypothesized that dGAG mice would exhibit widespread network disruptions compared to the cortex-specific EMX mice, due to broader TorsinA dysfunction across the basal ganglia and cerebellum. We also hypothesized that EMX mice would exhibit altered functional connectivity and activation patterns, supporting the idea that TorsinA dysfunction in the sensorimotor cortex alone can induce network abnormalities. In dGAG animals, we observed significantly lower functional connectivity between key sensorimotor nodes, such as the globus pallidus, somatosensory cortex, thalamus, and cerebellum. EMX mice, while showing less extensive network disruptions, exhibited increased functional connectivity between cerebellum and seeds in the striatum and brainstem. These functional connectivity alterations between nodes in the basal ganglia and the cerebellum in both dGAG, EMX models underscore the involvement of cerebellum in dystonia. No significant structural changes were observed in either model. Overall, these results strengthen the concept of dystonia as a network disorder

where multiple nodes across the brain network contribute to pathophysiology, supporting the idea that therapeutic strategies in dystonia may benefit from consideration of network properties across multiple brain regions.

KEYWORDS

DYT1 dystonia, cerebellum, cortex, basal ganglia, functional connectivity

Introduction

DYT1 dystonia is an early onset, generalized form of isolated dystonia characterized by sustained involuntary muscle co-contraction that results in abnormal movements and postures [1]. It is the most common form of hereditary dystonia and is caused by a heterozygous in-frame dGAG mutation in the TOR1A/DYT1 gene, which encodes the TorsinA protein [2]. The ΔGAG mutation results in functional alterations in TorsinA, potentially causing protein mislocalization [3], impaired interactions with other proteins, disrupted intracellular trafficking [4], and endoplasmic reticulum stress [5]. These disruptions can impair neuronal communications, particularly in brain regions with high TorsinA expression, such as the basal ganglia, cerebellum, and cerebral cortex [6].

Some studies hypothesize that dystonia can be viewed as a disorder primarily associated with basal ganglia dysfunction with abnormalities in the striatum [7, 8]. However, recent work supports the conceptualization of dystonia as a functional network disorder, where disrupted communication and integration of signals across multiple neural nodes contribute to its pathophysiology [9–12]. Alongside the basal ganglia, the cerebellum and cerebral cortex have been recognized as critical nodes in understanding dystonia. Studies show that the cerebellum can directly modulate basal ganglia activity through the cerebello-thalamo-basal ganglia pathway, leading to the hypothesis that dystonia may be driven by cerebellar dysfunction, which then alters basal ganglia output via this pathway [13, 14]. For instance, Fluorodeoxyglucose Positron Emission Tomography (FDG-PET) studies had reported increased glucose metabolism at rest in the cerebellum and supplementary motor area (SMA) of patients with sporadic and genetic dystonia [15]. Studies using diffusion tensor imaging (DTI) in DYT1 mutation carriers had found reduced fractional anisotropy in the subgyral white matter of the sensorimotor cortex [16] and abnormalities in white matter near cerebellum [17]. Moreover, Argyelan et al. (2009) also found that non-manifesting carriers had additional fiber tract disruptions along the thalamocortical region.

Research in transgenic animal models has deepened our understanding of TorsinA dysfunction. Dyt1 dGAG knock-in (dGAG) mice exhibit sustained electromyographic (EMG) potentials and intermittent co-contraction of muscle groups, mirroring one of the core features of human dystonia [18, 19]. FDG-PET studies in dGAG mice have shown increased regional metabolic activity in the cerebellar vermis, similar to findings in human patients [20, 21]. Some studies have also shown that dGAG mice display microstructural alterations in cerebellar circuitry [20, 22, 23]. Uluğ et al. 2011 found that fractional anisotropy in cerebellar efferent to the thalamus were negatively correlated with metabolic activity in sensorimotor cortex. This finding supports their hypothesis that inhibition of the cerebello-thalamo-cortical pathway plays a role in dystonia, as the loss of cortical inhibition is associated with increased neural activity. Nevertheless, studies with conditional deletion of Tor1A in forebrain cholinergic and GABAergic neurons [24], the striatum [25] or cortex [26], have exhibited motor dysfunction. Given that disruption of TorsinA in these other regions can result in motor deficits without direct TorsinA impact in the cerebellum, suggests that cerebellum may not be the sole origin point for dystonia-related motor deficits. Supporting this idea, prior work showed that although dopamine-2 receptors and Purkinje cell specific dGAG knock-in models both showed sensorimotor network alterations, only the dopamine-2 receptor model had motor deficits [27].

To bolster the framework for dystonia as a functional network disorder, a more comprehensive understanding of how TorsinA dysfunction in specific cell types contributes to alterations in network connectivity and dystonia-related pathophysiology is crucial. In this study, we aimed to elucidate the impact of TorsinA mutation globally and when torsinA mutation is restricted to the cortical and hippocampal neurons. To accomplish this, we utilized two distinct Dyt1 mouse models. The first model was a Dyt1 dGAG global knock-in with the mutation expressed throughout the body, impacting the entire brain, whereas the second model involved cerebral cortex-specific Dyt1 dGAG knock-in using the Emx1 promoter. In both models, we performed *in vivo* neuroimaging at ultra-high field (11.1T). We used functional magnetic resonance imaging (fMRI) to assess resting-state and sensory-evoked brain connectivity and activation, along with diffusion MRI (dMRI) to evaluate microstructural changes. We hypothesized that dGAG mice would exhibit widespread network disruptions due to torsinA dysfunction across all brain cells, including cortex, basal ganglia, and cerebellum. We also hypothesized that cortex-specific EMX mice would show network disruptions, supporting the idea that TorsinA dysfunction in the sensorimotor cortex alone can induce abnormalities, but that these would be less widespread due to sparing of cell types in basal ganglia and cerebellum.

Materials and methods

Animals

This study included two dystonic mouse models. In Model 1, we used an established mouse model with a knock-in of the same GAG trinucleotide deletion found in DYT1 dystonic patients, referred to as the dGAG model. Given that the homozygous GAG deletion (dGAG/dGAG) genotype is lethal in rodents, this dGAG model is heterozygous, possessing one normal Dyt1 allele and one allele with the GAG deletion throughout the body. Generation of this mouse model has been described in detail previously [18]. In Model 2, we developed cerebral cortex cell-specific Emx1-cre knock-in mice, which we designated as the EMX mouse model. This model was generated by introducing the Cre recombinase gene under the control of the EMX1 promoter, ensuring that Cre is expressed specifically in cerebral cortex and hippocampal neurons. This specificity allows for targeted genetic modifications in these cells within the cerebral cortex and hippocampus. The generation of this mouse model has previously been described in detail [28]. Emx1-cre heterozygous mice were bred with Tor1a^{Swap} heterozygous mice (Jackson Laboratory strain number 28099) [29] to generate Emx1-cre and Tor1a^{Swap} double heterozygous mice as experimental mice. Emx1-cre heterozygous littermates which carry the Cre allele but lack the dGAG mutation, were used as controls. These controls ensure that the experimental effects are due to selective mutation and not confounding factors such as genetic background or environmental influences. This design minimizes variability and allows for direct comparison within the same litter. Mice from both EMX cohorts were generated on the C57BL/6 background strain. In accordance with NIH policy of factoring in sex as a biological variable, we included both male and female mice in all groups. For the experiments we have used littermate control groups specific to each model, which is important to minimize the effects of the background strain and cage-to-cage variability on comparisons of mutant vs. control groups in each cohort. The dGAG cohort included 31 (male = 15, female = 16) mice with heterozygous Dyt1 dGAG knock-in mutation globally with mean age of 225 ± 25 days, and 29 control (male = 11, female = 18) mice with mean age of 229 ± 18 days. EMX cohort included 28 (male = 10, female = 18) mice with heterozygous Dyt1 dGAG conditional knock-in mutation in cortical and hippocampal neurons with mean age of 192 ± 24 days, and 36 control (male = 14, female = 14) mice with mean age of 200 ± 32 days. Experiments were performed in accordance with NIH guide for care and use of laboratory animals (NIH Publications No. 8023, revised 1978). All animals were maintained on a 12/12 h light/dark cycle with food and water *ad libitum*. All experiments were approved and monitored by the University of Florida Institutional Animal Care and Use Committee.

Experimental design

Four types of MRI scans were acquired for every animal: an anatomical, a sensory-evoked fMRI, resting-state fMRI, and diffusion MRI. Experimenters performing MRI scans were blind to which animals belonged to the experimental or control groups for each model. After testing and data preprocessing were completed blinded to genotype, genotyping was performed by Polymerase Chain Reaction method on tail clips. Experimenters were then unblinded to enable group-wise comparisons. Animal data were excluded only due to technical issues encountered during data processing. For resting state fMRI, 1 dGAG cohort animal and 3 EMX cohort animals were excluded due to challenges in CSF segmentation during processing. The technical difficulties prevented reliable analysis of the affected data. Importantly, no animal data were removed from sensory-evoked fMRI or diffusion MRI analyses. Methods for each stage of this study are described in detail in the following sections.

MRI preparation and scan parameters

Before animals were taken for MRI scans, animal preparation was performed as previously described [30]. Animals were initially put into an enclosed chamber under brief administration of 3% isoflurane delivered through a vaporizer (SurgiVet, Dublin, OH) connected to a charcoal trap. Anesthesia was maintained between 1 and 1.5% for the remaining experimental duration to accommodate necessary vitals and motion considerations. The experimental setup has previously been illustrated [27, 30]. Mice were placed in a prone position on a custom 3D platform equipped with a bite bar that immobilized the head and delivered anesthesia. A respiration pad (SA instruments, Stony Brook, NY) was placed under the abdomen of the animals to monitor respiration throughout the imaging. Core body temperature was maintained using an in-house recirculating waterbed heating system and monitored via a thermal rectal probe (SA instruments, Stony Brook, NY). An MR compatible advanced thermal stimulator (ATS) thermode (PATHWAY System, Medoc Advanced Medical Systems, Ramat Yishay, Israel) was affixed to right planter hind paw, to deliver heat stimulation during imaging.

MRI data were acquired on an 11.1 T Magnex Scientific 40 cm horizontal magnet (Agilent, Inc. Palo Alto, CA, United States) with RRI BFG-240/120-S6: bore size 120 mm, Gmax = 1,000 mT/m @325A with 200 μs rise time. B1 excitation and signal detection were achieved using an in-house 2.5 × 3.5 cm quadrature surface transmit/receive mouse head coil tuned to 470.7 MHz (1H resonance) (AMRIS, University of Florida). Scan sequences were prepared and controlled using ParaVision, Version 6.0.1 (Bruker BioSpin, Billerica, MA).

Anatomical T2-weighted images were acquired for spatial normalization using a turbo RARE sequence with the following parameters: TR = 5500 ms; TE = 30 ms; excitation angle = 90°; refocusing angle = 180°; dummy scans = 1; averages = 7; slices = 13; orientation = coronal; thickness = 0.9 mm; gap = 0 mm; FOV = 15 × 15 mm; data matrix = 256 × 256 in-plane.

Sensory-evoked and resting-state fMRI scans were acquired using a 2-shot EPI sequence with the following parameters: TR = 2000 ms; TE = 15 ms; repetitions = 360 (sensory-evoked fMRI) or 180 (resting-statefMRI); flip angle = 90°; dummy scans = 2; slices = 13; coronal orientation; thickness = 0.9 mm; gap = 0 mm; FOV = 15 × 15 mm; data acquisition matrix = 64 × 64 in-plane.

Diffusion MRI scans were acquired using an EPI sequence with the following parameters: TR = 4,000 ms; TE = 19 ms; averages = 4; flip angle = 90°; slices = 17; orientation = coronal; thickness = 0.7 mm; gap = 0 mm; FOV = 15 × 11 mm; data matrix = 128 × 96 in-plane. The following diffusion parameters were used: two non-diffusion weighted b0 images and 52 diffusion-weighted directions (6 directions at b = 600 s/mm^2 and 46 directions at b = 2000 s/mm^2).

Sensory-evoked fMRI thermal stimulation paradigm

The acquisition of sensory-evoked fMRI was conducted using heat-induced stimulation of the right plantar hind paw. The PATHWAY System was calibrated to deliver thermal stimulation in a block paradigm, alternating between 60 s at the stimulation temperature (42°C) and 60 s at the baseline temperature (30°C), beginning and ending with a 30 s baseline block. Temperature transitions between blocks were accomplished within 300 milliseconds, with cooling and heating rates of 40°C/s and 70°C/s, respectively.

fMRI processing and analysis

Data processing for sensory-evoked and resting state fMRI scans were preformed using custom-designed UNIX shell scripts with commands from FMRIB Software Library (FSL: Oxford, UK), Analysis of Functional Neuro-Images [31] and Advanced Normalization Tools [32]. The fMRI processing pipeline was automated and applied equally and without bias to all scans. We acquired duplicate scans for resting-state fMRI and concatenated the data such that resting-state data were analyzed as a single time series. Data were only excluded from the fMRI analyses due to excessive motion that prevented deconvolution of the hemodynamic response function.

The first 5 TRs were removed from the time series to account for magnetization equilibrium. Outliers within each voxel's time series were identified using 3dToutcount in AFNI, and volumes with >5% of the total voxels identified as outliers were flagged and were excluded during regression. Scan data were then de-spiked, slice-time corrected, corrected for motion and distortion via alignment to the first volume (3dvolreg, AFNI), spatially smoothed with a 0.3 mm full width half maximum (FWHM) Gaussian kernel, and scaled to have a range of (0, 200) and mean of 100. Brain masks were created on high resolution anatomical images and affine registered to fMRI scan from the same animal to remove signal from voxels outside the brain. Six motion parameters from the motion correction step (three translational and three rotational) were included as demeaned motion parameters in the sensory-evoked fMRI regression model. Given the subtle nature of resting state fMRI, additionally, first-order derivatives of these motion parameters were also incorporated into the regression model for resting-state fMRI analysis. Including these twelve parameters (six motion parameters and their derivatives) in the regression model has been suggested to improve resting-state functional connectivity analysis [33].

To spatially normalize data, fMRI images from each mouse were registered to the T2-weighted anatomical scan from the same animal, and then to a high-resolution T2-weighted mouse template brain, generated from anatomical scans of 160 mice [34]. A total of 23 *a priori* selected seed regions-of-interest in the brain were drawn (shown in Figure 1) on the template image in both hemispheres from 12 anatomical locations (11 bilateral anatomical regions, except vermis). Seeds were drawn with reference to the Allen Mouse Brain Atlas, a high-resolution coronal anatomic reference atlas with a systematic, hierarchically organized taxonomy of mouse brain structures[1]. Small seeds were employed to ensure spatial specificity, minimize overlap with adjacent regions, and focus on distinct functional connectivity patterns. For larger brain regions such as the striatum, thalamus, and midbrain, seeds were carefully placed within subregions that are functionally relevant to dystonia. This approach is consistent with commonly accepted practices in seed-based functional connectivity analysis. For group level analyses, to constrain the analysis only in dystonia related sensory-motor network, we have manually drawn the seed regions and the brain mask according to Allen Reference Atlas-Mouse Brain[2] (Supplementary Figure S1) that included relevant brain regions (including cerebellum, vermis, medulla oblongata, pons, midbrain, thalamus, cortex, striatum).

Sensory-evoked fMRI analysis

Stimulation-induced hemodynamic response time series was modeled using the hemodynamic response function convolved

1 https://mouse.brain-map.org/static/atlas

2 atlas.brain-map.org

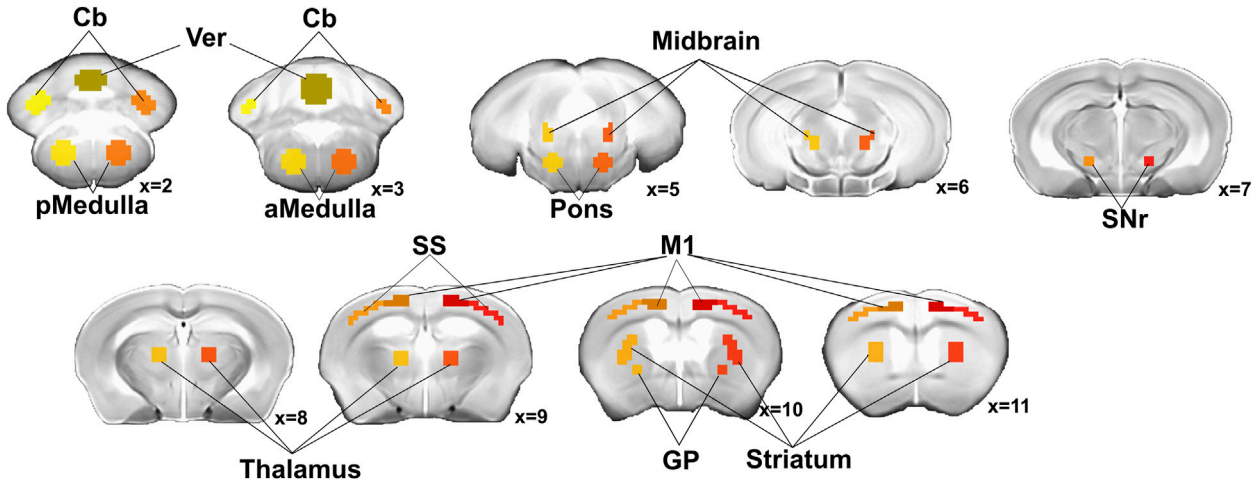

FIGURE 1
Seeds are overlaid on a T2-weighted mouse template brain. A total of 23 seeds are displayed. Seeds in the left hemisphere are shown in yellow shades, while those in the right hemisphere are depicted in red shades. The unilateral vermis is illustrated in brown. The seeds include the cerebellum (Cb), posterior medulla, anterior medulla, pons, midbrain, substantia nigra (SNr), thalamus, globus pallidus (GP), somatosensory cortex (SS), primary motor cortex (M1), and striatum, separately for the left and right sides of the brain, as well as the vermis.

with BLOCK basis function with amplitude 1 and spanning 60s from onset of each stimulation. Using 3dDeconvolve in AFNI, the regression was performed across baseline and stimulation blocks to estimate β-coefficient and its associated t-statistic for the BOLD Contrast. Two separate analyses were performed [1]: examination of thermal stimulation induced blood-oxygen level dependent (BOLD) response and [2] a seed-based BOLD correlation analysis to examine functional connectivity in response to thermal stimulation. We utilized the AFNI 3dMVM function [35] to conduct a group-level ANOVA-style statistical analysis on the β-coefficient of each voxel, incorporating group and sex as interaction terms among the between-subject variables. Since all the animals were in a narrow age range, age was not included as a factor in the statistical model. We used the sensory-motor mask to constrain the analysis within the dystonia relevant brain region. Group effects were considered significant at $p < 0.05$ (FWER corrected). In order to control false-positives across voxels, AFNI 3dttest++ function with the 3dClustSim option was utilized to obtain cluster-level threshold, which performs Monte Carlo simulation to estimate the probability of obtaining clusters of a certain size through randomization and permutation simulations. The ClustSim cluster-level significance threshold determines the minimum number of significant (uncorrected) voxels required for a cluster to be considered significant, effectively controlling for false positives at our desired alpha level of 0.05 [36]. This method is functionally analogous to other approaches used for controlling multiple comparisons. ClustSim calculations were performed separately for the EMX and dGAG cohorts using the voxel-level threshold of $p < 0.01$ (uncorrected) with a nearest neighbor, NN = 3, bi-sided clusterization. Functional connectivity was analyzed by examining the entire sensory-evoked fMRI time-series across baseline and stimulation blocks using a seed-based correlation approach. From the residual time series as output from 3dDeconvolve, Pearson's correlation coefficients were computed between the time series of the seeds and brain voxels in whole brain. Correlation coefficients were converted to Z-scores using Fisher r-to-z transformations. We analyzed these Z-scores for group level functional connectivity analysis using 3dMVM function, incorporating group and sex as main factor and their interaction term as between-subject variable in the statistical model. We further performed post-hoc t-tests to identify genotype effects in male and female subsets for each model. We used the sensory-motor brain area as a mask to constrain the analysis within the mask area. ClustSim calculations were performed separately for the EMX and dGAG cohorts using the voxel-level threshold of $p < 0.01$ (uncorrected) with nearest neighbor (NN = 3), bi-sided clusterization.

Resting-state fMRI analysis

Concatenated and preprocessed resting-state fMRI data were subjected to general linear regression analysis. Volumes flagged for excessive motion by 3dToutcount were censored and excluded from the regression analysis. Then, we applied additional regressors for the mean signal from cerebrospinal fluid (CSF) and the first-order derivatives of the motion parameters (six motion parameters and their derivatives,

twelve motion parameters in total) calculated during motion correction. Next, we performed seed-to-voxel resting-state functional connectivity analysis. We extracted the mean signal of all voxels within each 23 ROIs for each time point in the concatenated time series, which was then correlated with the time series of each voxel throughout the brain to generate a whole brain map of functional connectivity. We performed a voxel-wise ANOVA test using 3dMVM function to identify between group effects for both cohorts, incorporating group, sex as an interaction factor in the model. We performed post-hoc t-tests to identify genotype effects in male and female subset for each model. We included sensory-motor brain mask for analysis within the relevant brain area. Group effects were considered significant at $p < 0.05$ (FWER corrected). For the cluster level, same as sensory-evoked fMRI analysis, 3dttest++ ClustSim option were used for $p < 0.01$, NN = 3, bi-sided clusterization was used for group level statistics.

Diffusion MRI processing and analysis

Data processing for diffusion MRI was performed using custom-designed UNIX shell scripts with commands from AFNI, FSL, MRTrix3 [37] and ANTs [32]. The diffusion MRI processing pipeline was automated and therefore, could be applied to all the scans equally and without any bias. As the first step, the "dwidenoise" function from MRTrix3 was used to denoise the diffusion data [37, 38, 39]. Next, the "mrdegibbs" function from MRTrix3 was used to mitigate Gibbs ringing artefacts from the data [40]. B0 images were then extracted from the scan data and the 3dAutomask function from AFNI, with options customized for diffusion data, was utilized to generate a mask that separated brain tissue from non-brain tissues. The scan data were then processed using the MRTrix3 function "dwifslpreproc," which implements FSL's Topup and Eddy workflows to correct for susceptibility and eddy current-induced distortions, and replaces outliers caused by signal dropouts due to subject motion [41–43]. Subsequently, bias field correction was performed using the "dwibiascorrect" function from MRTrix3 [37]. As the final step of preprocessing, spatial smoothing was applied with Gaussian kernal with a FWHM of 0.2 mm. Diffusion parameters were estimated from the multi-shell diffusion data using a two-compartment model to account for partial volume effects of extra-cellular free-water [44, 45], implemented as a part of open-source software package Diffusion Imaging in Python [46]. Resultant maps of free-water (FW) and free-water corrected FA (FWC-FA) were variables of interest for this analysis.

To spatially normalize the data, FWC-FA images from each mouse were nonlinearly registered in a slice-by-slice manner to an FWC-FA mouse template brain, generated from FWC-FA maps of 160 mice. This helped us prevent possible warping due to the high in-plane resolution (117 × 115 μm) and accommodate the relatively large slice thickness (700 μm) of the diffusion scans [34].The transformation matrices derived from registration of the FWC-FA scans to the template were then applied to the FW image from the same animal. For analyzing the group differences, we performed ANOVA style statistical test using 3dMVM, incorporating group, sex as the main factors and their interaction as between-subject variable in the statistical model. Statistics were performed separately for FW and FWC-FA. Group effects were considered significant at $p < 0.05$ (FWER corrected). For the cluster level, same as fMRI analyses, 3dttest++ with ClustSim option were used for $p < 0.01$, NN = 3, bi-sided clusterization was used for group level statistics.

Results

dGAG animals imaging findings

No sensory-evoked BOLD activation differences in dGAG

We performed voxel-wise analysis of BOLD activation in response to sensory stimulation in dGAG mice and controls. We observed no significant BOLD differences between the dGAG cohort and the control animals. There was significant main effect of sex for BOLD activation in cerebellum and midbrain (caudo-medial) areas, however these sex differences were similar in both dGAG and control mice, as no genotype by sex interaction in BOLD activation were observed. There were no significant differences in genotype for male or female subsets.

Region-specific differences in sensory-evoked functional connectivity in dGAG

We performed sensory-evoked functional connectivity analysis and observed several seed regions that showed lower functional connectivity during the sensory-evoked paradigm in dGAG animals compared to controls (Figure 2A). Specifically, the seed in left globus pallidus (Gp) showed significantly lower functional connectivity with right somatosensory cortex (SS) and right cerebellum. The seed in left thalamus showed significantly lower functional connectivity with the right somatosensory cortex, left thalamus, and left midbrain (caudo-lateral region). Additionally, the seed in right somatosensory cortex showed significantly lower functional connectivity with the right thalamus. The seed in right thalamus showed significantly lower connectivity with the right midbrain (caudo-lateral region). The seed in right substantia nigra (SNr) showed significantly lower functional connectivity with the left thalamus.

There were many seed to brain functional connectivity that showed a main effect of sex, observed across both the dGAG and control mice. We observed a genotype-by-sex interaction in the left Gp seed to cerebellar vermis. Post-hoc analysis of the male subset showed several significant differences in functional connectivity compared to the control animals. The seed in vermis showed significantly lower functional connectivity with thalamus. Similarly, the seed in the left anterior medulla showed

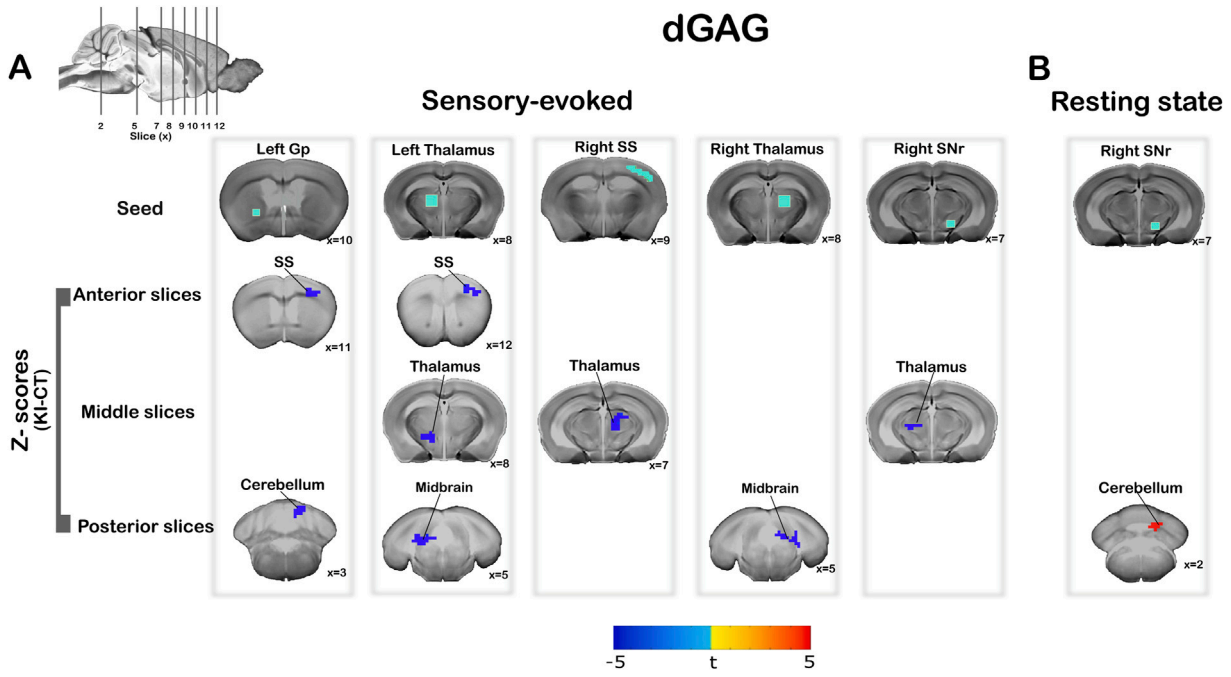

FIGURE 2
Sensory-evoked and resting state functional connectivity for dGAG cohort. Coronal slices on the top row show seed regions in turquoise color and columns below each seed show significant group difference (KI-CT) in functional connectivity. **(A)** Shows sensory-evoked functional connectivity. **(B)** Shows resting state functional connectivity. Statistical significance was determined using 3dClustSim with a voxel-wise $p < 0.01$ (uncorrected) and FWER-corrected cluster threshold at $p < 0.05$. Clusters that passed $p < 0.05$ threshold (FWER corrected) are showed in blue and red color. The intensity of the color reflects the magnitude of the group difference, indicated by the corresponding t values (scale is provided by color bar). Here, blue colors represent lower functional connectivity in dGAG mice, and red colors represent higher functional connectivity in dGAG mice. The sagittal mouse brain on the top left provides the location of the coronal slices corresponding to the brain areas with significant functional connectivity differences. Here SS, Somatosensory cortex; Gp, Globus pallidus; SNr, Substantia Nigra.

lower connectivity with primary motor cortex. Reduced connectivity was also observed between the seed in left somatosensory cortex and thalamus, as well as between the seed in right cerebellum and the midbrain. The seed in right somatosensory cortex showed significantly lower functional connectivity with both cerebellum and thalamus. Additionally, the seed in right posterior medulla and the seed in right somatosensory cortex both showed significantly lower functional connectivity with cerebellum. Lastly, the seed in right substantia nigra showed lower connectivity with somatosensory cortex. In contrast, post-hoc analysis of female subset showed the seed in right substantia nigra showed significantly higher functional connectivity with somatosensory cortex. We summarized the significant effects of genotype, sex and their interaction, male and female only genotype difference in Supplementary Table S1 in Supplementary Material.

Region-specific differences in resting state functional connectivity in dGAG

Similar to sensory-evoked functional connectivity analysis, we performed connectivity analysis for resting state fMRI and investigated genotype, sex differences and genotype-by-sex interaction. For the seed in right substantia nigra, there was significant higher functional connectivity with the right cerebellum (Figure 2B). There were no sex differences and no genotype-by-sex interaction for resting state functional connectivity in dGAG mice. Post-hoc analysis of male subset showed significantly lower functional connectivity between seed in right cerebellum and midbrain, and seed in right midbrain with cerebellum. In contrast, there was no significant functional connectivity differences in the female subset. We summarized the significant effects of genotype, sex and their interaction, male and female only genotype difference in Supplementary Table S2 in Supplementary Material.

No genotype differences were observed in diffusion MRI for the dGAG cohort

We performed voxel-wise analysis of FW and FWC-FA to compare dGAG animals with controls. There were no significant group differences between dGAG mice and control for either FW or FWC-FA. Further we analyzed if there was any sex differences and genotype by sex interaction in the dGAG animals. There was a significant main effect of sex in FWC-FA, with male animals

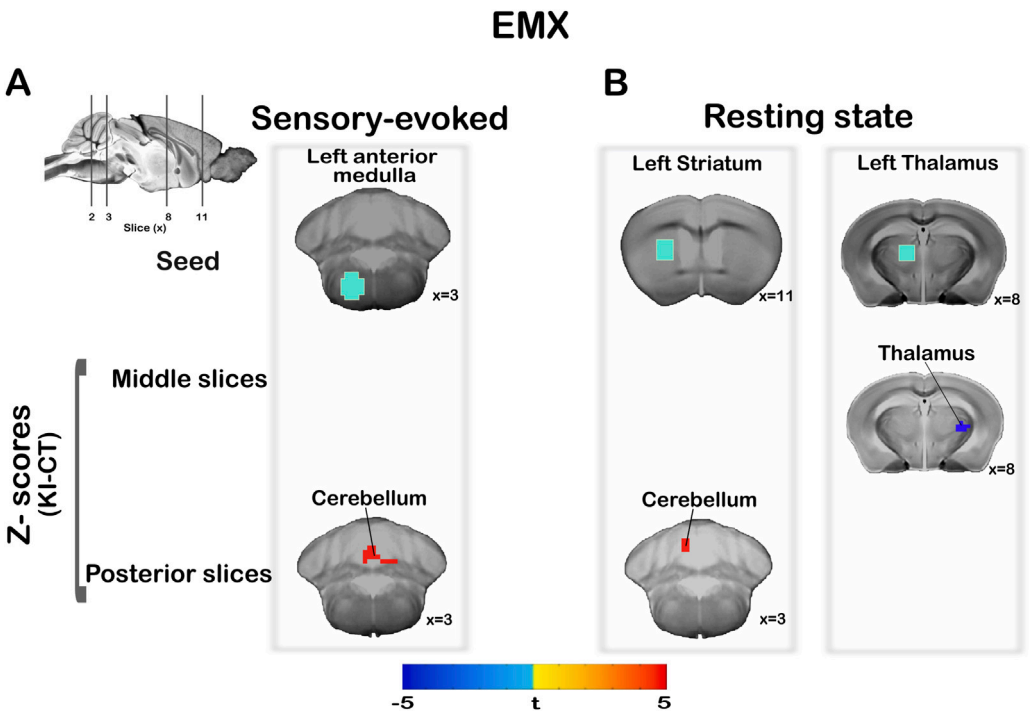

FIGURE 3
Sensory-evoked and resting state functional connectivity for EMX. Coronal slices on the top rows present the seed regions in turquoise color and bottom rows are showing voxel clusters with significantly different t scores between EMX and control animals. Statistical significance was determined using 3dClustSim with a voxel-wise $p < 0.01$ (uncorrected) and FWER-corrected cluster threshold at $p < 0.05$. Clusters that passed $p < 0.05$ threshold (FWER corrected) are showed in blue and red color. The intensity of the color reflects the magnitude of the group difference, indicated by the corresponding t values (scale is provided by color bar). **(A)** Shows sensory-evoked functional connectivity difference between seed regions and brain areas inside sensory-motor cortex network, where blue color represents lower degree of functional connectivity. **(B)** Shows resting state functional connectivity differences between regions and brain areas in sensory motor networks. Red represents a high degree of functional connectivity. The sagittal image on the leftmost corner of the figure shows slices corresponding to the brain areas with significant functional connectivity differences.

with higher FWC-FA in superior colliculus, but these differences were similar in both dGAG and control animals as there were no significant genotype-by-sex interactions. Post-hoc analysis with male and female subset showed no significant difference in FW or FWC-FA, compared to the control animals.

EMX imaging findings

No sensory-evoked BOLD activation differences in EMX

Similar to dGAG animals, we performed voxel-wise analysis of BOLD activation in response to sensory stimulation in EMX animals. There were no significant BOLD differences between the EMX knock-in and the control animals. We further analyzed sex differences and genotype by sex interaction and there were no significant differences in either for BOLD activation. Post-hoc analysis with male and female subset separately also showed no significant differences in genotype.

Region-specific differences in sensory-evoked functional connectivity in EMX

We analyzed sensory-evoked functional connectivity analysis in EMX animals. For the seed in left anterior medulla, there was significantly higher functional connectivity to the midline cerebellum (Figure 3A). Many seeds showed a main effect of sex on functional connectivity; however, these sex differences were observed in both EMX and control mice, and only the seed right pons showed a genotype-by-sex interaction to the cerebellum. Post-hoc analysis in the male subset showed significantly higher connectivity between seed in left striatum and cerebellum and between seed in right posterior medulla and midbrain. Whereas, for the female subset, there was significantly lower functional connectivity between seed in right posterior medulla and cerebellum. We summarized the significant effects of genotype, sex and their interaction, male and female only genotype difference in Supplementary Table S3 in Supplementary Material.

Region-specific differences in resting state functional connectivity in EMX

Similar to sensory-evoked functional connectivity analysis, we performed connectivity analysis for resting state fMRI and investigated genotype differences, as well as sex differences and genotype-by-sex interaction. For the seed in left striatum, there was significantly higher functional connectivity with cerebellum (Figure 3B). Whereas there was significantly lower functional connectivity between the seed in left thalamus and right thalamus.

There was a significant sex differences between the seed in left striatum and cerebellum, but there were no genotype-by-sex interactions. Post-hoc analysis of male subsets showed there was significantly higher functional connectivity between the seed in left striatum and cerebellum and lower connectivity between seed in right posterior medulla with midbrain. In contrast, for female subset, there was significantly lower functional connectivity between the seed in right posterior medulla and cerebellum and between the seed in right somatosensory cortex and anterior medulla. We summarized the significant effects of genotype, sex and their interaction, male and female only genotype difference in Supplementary Table S4 in Supplementary Material.

No genotype differences were observed in diffusion MRI for the EMX cohort

We performed voxel-wise analysis for FW and FWC-FA to compare EMX animals with controls. There were no significant group differences between EMX mice and controls for either FW or FWC-FA. Further we analyzed if there was any sex differences and genotype by sex interaction in the EMX animals. There was significant main effect of sex in FWC-FA, with male animals having higher FWC-FA in cerebellum, but these differences are similar in both EMX and control animals as there were no significant genotype-by-sex interactions. Post-hoc analysis for male and female subset separately showed no significant difference.

Discussion

The emerging view of dystonia as a network disorder suggests that multiple nodes in the brain including the basal ganglia, cerebellum, and cerebral cortex are involved in its pathogenesis. While decades of research have highlighted a central role for the basal ganglia in dystonia, the involvement of the cerebellum and cerebral cortex has also been increasingly recognized. However, the mechanisms through which these nodes interact and contribute to broader pathophysiology of dystonia remains unclear and warrant further investigation.

In the present study, we utilized two transgenic mouse models to investigate the neural underpinnings of dystonia: one model expressing a widespread DYT1 mutation globally, and another with a cortex and hippocampal neuron specific DYT1 mutation. We conducted *in vivo* fMRI and dMRI to assess the functional connectivity and structural integrity of the sensorimotor network. Although dystonia is classically defined by motor symptoms, it also involves sensory deficits, including impaired sensory-motor integration [47, 48]. We utilized a sensory-evoked fMRI paradigm to drive sensorimotor network activity, building on prior work demonstrating its sensitivity in characterizing subtle sensorimotor network dysfunction [27, 30, 34].

We observed significant differences in functional connectivity during sensory-on versus sensory-off periods in mutant animals in both the dGAG and EMX cohorts. There was significantly lower functional connectivity between key sensorimotor nodes, such as the globus pallidus, somatosensory cortex, thalamus, and cerebellum in dGAG animals. This pattern of reduced connectivity may suggest impaired sensory integration and weakened modulatory influences between the basal ganglia and cerebellum, potentially disrupting the communications critical for motor control. We found reduced connectivity between the thalamus and cortex in both directions (seed in thalamus to cortex and seed in cortex to thalamus) which strengthens the idea of disrupted communication within these nodes in sensorimotor network. Neuroimaging studies in humans found reduced cerebello-thalamic connectivity in TorsinA mutation carriers and additional disruptions in the thalamo-cortical pathway in non-manifesting carriers [17, 21]. A study with dGAG knock-in mice also exhibited cerebellothalamocortical motor pathway abnormalities, similar to human non-manifesting gene carriers [20]. The reduced connectivity between thalamus and somatosensory cortex in our knock-in animal model aligns with the findings and reinforces the idea that thalamo-cortical pathway contributes to the pathophysiology of dystonia [49]. Interestingly, we also found significantly lower connectivity from the substantia nigra to the thalamus and higher connectivity from substantia nigra to the cerebellum in dGAG animals. This pattern might indicate a compensatory shift, where the cerebellum might take a more prominent role in motor coordination due to reduced basal ganglia output via thalamocortical connections. The increased connectivity may represent an adaptive process that aimed at mitigating motor deficit, where cerebellum potentially acting as a compensatory hub to maintain the functional network integrity despite disruptions in basal ganglia.

In the EMX cohort we also observed altered functional connectivity, although less extensive than in the dGAG cohort. EMX mice demonstrated increased functional connectivity from the anterior medulla to cerebellum and striatum to the cerebellum. It is noteworthy that although TorsinA mutation was constrained to cerebral cortex and hippocampal neurons alone in EMX animals, functional connectivity alterations were observed downstream from the

cortex, impacting subcortical dynamics between the basal ganglia and cerebellum.

These functional connectivity alterations between nodes in the basal ganglia and the cerebellum in both dGAG and EMX cohorts highlight the role of cerebellum in dystonia, even when TorsinA mutation is isolated to cell-specific neurons in the brain. Impaired cortical input can have significant effects on cerebellar signaling since cerebellum relies on input from the cerebral cortex for motor learning, adjustment of movement, and error correction using an internal model [50]. This disruption can impair cerebellar functions such as updating motor commands and integrating sensory feedback, leading to motor deficits and movement disorders like dystonia or ataxia. A study with pharmacological mouse model of rapid-onset dystonia demonstrated that cerebellum communicates with basal ganglia with a short latency, bi-synaptic pathway to modulate the activity of striatum. This study provides one plausible explanation that under pathological conditions, this pathway allowed transferring the aberrant cerebellar activity to basal ganglia and can cause dystonic movements [13]. Similarly, a recent study with manifesting dystonic patients reported that there was a gain of connections between core nodes in dystonia (i.e., cerebellum, basal ganglia, thalamus and different parts of cortex [49]. Findings from the present study of disrupted functional connectivity across various nodes in the cortex, basal ganglia, thalamus, and cerebellum underscore the notion of dystonia as a broader network disorder, rather than primary dysfunction from a single node in the brain.

We observed a significant main effect of sex in functional connectivity for both dGAG and EMX animals. Genotype-by-sex differences showed significant connectivity alterations from seed Gp to vermis in dGAG animals, suggesting that TorsinA dysfunction impacts basal ganglia-cerebellar communication differently in male and female Dyt1 animals. We found male dGAG animals had lower functional connectivity than female animals for the knock-in group, which was the opposite what we observed in the control group. Male dGAG animals demonstrated functional alteration between many key regions in the brain compared to control males. Notably, there was functional alteration from seeds in primary motor cortex, medulla, and right somatosensory cortex to cerebellum. In addition, there was significantly reduced connectivity between cerebellum and midbrain in both directions (seed in cerebellum to midbrain and seed in midbrain to cerebellum). In contrast, female dGAG animals showed only a single instance of higher functional connectivity compared to control females, which was between the seed in substantia nigra to somatosensory cortex. These findings suggest that male dGAG mice experience more widespread disruptions in key sensorimotor and cerebellar circuits, which is consistent with previous reports of greater severity and earlier onset of motor symptoms in male compared to female dystonic patients [51].

In EMX animals, we also found sex-dependent alterations in functional connectivity. Analysis of EMX male only group demonstrated lower functional connectivity between seed in posterior medulla to midbrain. Alongside, there was significantly higher connectivity between seed in left striatum to cerebellum. In the female only group, there was significantly lower connectivity between the seed right posterior medulla with cerebellum and seed in right somatosensory cortex with anterior medulla. These findings suggest that the neural circuitry disruptions associated with the EMX model manifest differently between sexes. Although the number of seeds showing group differences in both sexes were similar, the pattern of changes were different. Males showed a combination of reduced and enhanced connectivity patterns, while females showed predominantly reduced connectivity. These findings may point to complex genotype-specific and sex-based influences on dystonia pathophysiology and further emphasizes the variability between male and female animals, which may impact the sensitivity to detect subtle differences. Since most dystonia research in animal models has predominantly focused on males, the role of sex in modulating genotype-specific effects remains underexplored. Future studies incorporating both sexes will be essential to elucidate these interactions and to provide a more comprehensive understanding of dystonia. The broader perspective could also help refine treatment approached and could provide key insights into variability in disease expression and response to treatments.

The present study showed no significant differences in sensory-evoked BOLD activation in either dGAG or EMX animal models. In prior work, TorsinA knock-out model targeting dopamine-2 receptors exhibited significantly reduced BOLD activation in the striatum, thalamus, and sensorimotor cortex, while knock-out model targeting cholinergic neurons showed reduced BOLD activation in the midbrain [30]. Similarly, knock-in model targeting dopamine-2 receptors demonstrated diminished activation in the somatosensory cortex, and knock-in model targeting Purkinje cells showed significantly reduced activation in the striatum and midbrain [27]. In human DYT1 patients, previous studies have demonstrated a multilevel loss of neuroaxis inhibition and increased cortical excitability [52, 53] and regional overactivation in the cerebellum has been consistently observed in DYT1 mutation carriers, regardless of clinical penetrance [53]. One possible explanation for the lack of detectable differences in this study is that in the dGAG model, where there is a brain-wide TorsinA dysfunction, the mutation may have more distributed effects whereby regional activity patterns may be influenced by compensatory signals from other nodes in the network, potentially masking specific, localized changes in BOLD activity. The widespread effects of the mutation could lead to compensatory mechanisms distributed in multiple brain regions, effectively diluting region-specific alterations in BOLD responses. In the EMX model, the cortex-specific mutation may not have been sufficient to

disrupt key cortico-cerebellar or basal ganglia circuits to the extent required for detectable fMRI changes. It is possible that the localized nature of the mutation affects only certain pathways, without producing the global network disruptions necessary to elicit measurable differences in BOLD activation. Previous study with EMX knock-out animals have reported well-preserved whisker-related patterns in the somatosensory cortex, which suggests that synapse formation and neural circuitry remain largely unaffected for these animals [26]. However, another study discussed neurodegeneration in brain structures for EMX-cre knock-out animals where torsinA was selectively deleted [54]. This discrepancy highlights the complexity of this model and suggests that specific experimental conditions, such as the methods used for assessing neural circuitry and tissue integrity, may influence the observed outcomes. In our study, both male and female mice were included in the experiment, which might have introduced variability in the data. Many prior studies in animal models of dystonia have been conducted primarily in male animals [30, 55–57]. In this study we observed sex-specific differences in functional connectivity in both dGAG and EMX models, highlighted in Supplementary Tables S1–S4. These differences may contribute to data variability, reducing the ability to detect consistent changes in BOLD activation.

Despite functional alterations observed in the present study, no significant structural changes were observed in either dGAG or EMX animals. Previous studies have reported structural alteration in cerebellum, basal ganglia and other components of sensorimotor network in clinical populations with dystonia [16, 17, 58, 59]. Microstructural differences have also been reported in basal ganglia and cerebellum in Dyt1 dGAG KI animals [20, 55, 60, 61]. As we speculated in our previous publication, this could be because of a relatively larger slice thickness (0.7 mm) that we used for our *in vivo* diffusion imaging compared to *ex vivo* dMRI, which allows longer scan times and higher spatial resolution. A previous diffusion MRI study of dGAG mice, using a bi-tensor model and similar slice thickness, revealed free water changes in both the basal ganglia and cerebellum [55]. In the present study, we included male and female mice, whereas in the DeSimone et al. (2016) study the authors included only male animals and thus the findings could have had more robust differences. Supporting this idea, we observed a significant main effect of sex on FWC-FA in the dGAG cohort (including mutant and control mice), which might contribute to the variability in the data and impact our ability to detect genotype differences.

The key focus of the study is to comprehensively characterize structural and functional alterations in dGAG and EMX animal models. While the study did not include direct behavioral assessments, the impact of TorsinA mutations on motor behavior has been extensively characterized, including global models and models targeting the cortex [18, 26, 62, 63]. It is possible that the functional connectivity alterations observed here may represent changes associated with motor behavior outcomes or may represent compensatory changes in sensorimotor circuits. These studies could provide a foundation for interpreting the connectivity changes observed here, linking them to established motor and behavioral phenotypes. By focusing on the neural alterations in these models, our work complements and extends the understanding of dystonia-related pathology. Future work may benefit from techniques such as optogenetics, to directly link the consequences of changes to these circuits to motor behavior in dystonia mouse models.

Overall, our finding indicates a greater degree of functional impairment in dGAG animals, which have the same heterozygous mutation as human DYT1 dystonia patients. Cortex-specific disruption of TorsinA in EMX animals was sufficient to elicit changes in important downstream regions in the basal ganglia and cerebellum, but these changes were constrained to fewer components within the larger sensorimotor circuitry. These findings serve the growing body of knowledge on the pathophysiology of dystonia and may help in establishing additional targets for therapeutic intervention. One of the reasons for the complexity of treating DYT1 dystonia is heterogeneity between patients, as treatments that benefit some individuals may not work for others. One explanation could be that TorsinA dysfunction differentially impacts nodes in the sensorimotor network. Therefore, identifying alterations across the larger sensorimotor network is essential. Prior work using cell-specific knock-in separately in the basal ganglia and cerebellum were also sufficient to induce functional changes in the sensorimotor network. The dGAG model from this paper and basal ganglia targeted D2-receptor knock-in from prior work [27] show more widespread dysfunction across many components of the sensorimotor network while using sensory-evoked fMRI paradigm. Although the cortex-specific EMX mice from this study and cerebellum specific PCP2 mice [27] showed alterations in important components of the sensorimotor network, those alterations were constrained to relatively fewer nodes in the sensorimotor network. The notion of brain-wide impact across multiple networks in dystonia might also help to explain why treatments like deep brain stimulation targeting globus pallidus don't work the same way for all patients. For individuals who are unresponsive to pallidal stimulation, targeting other regions such as the cerebellum or cortex could offer alternative therapeutic avenues. Multiple studies and case reports showed that stimulation in deep cerebellar nuclei significantly improved dystonia symptoms [64–66]. Motor cortex stimulation has shown promise in patients with primary fixed dystonia who were unresponsive to pallidal stimulation [67]. The present findings strengthen the concept of dystonia as a network disorder where multiple nodes across the brain contribute to its pathophysiology and highlight the idea that multiple brain regions may need to be considered for individualized therapeutic strategies in dystonia.

Data availability statement

The raw data supporting the conclusions of this article will be made available by the authors, without undue reservation.

Ethics statement

The animal study was approved by University of Florida Institutional Animal Care and Use Committee. The study was conducted in accordance with the local legislation and institutional requirements.

Author contributions

DV and YL conceptualized the experiment. YL and PG generated the animal models and managed animal colony. RA and BW collected data. RA, BW, and DV analyzed data, interpreted findings, and wrote the manuscript. RA, BW, PG, YL, and DV all contributed edits and revisions to the final manuscript. All authors contributed to the article and approved the submitted version.

Funding

The author(s) declare that financial support was received for the research, authorship, and/or publication of this article. This work was supported by the National Institutes of Health (Project Numbers R01NS075012 and R01NS129873). A portion of this work was performed in the McKnight Brain Institute at the National High Magnetic Field Laboratory's Advanced Magnetic Resonance Imaging and Spectroscopy (AMRIS) Facility, which is supported by National Science Foundation Cooperative Agreement No. DMR-1644779 and the State of Florida. This work was also supported in part by an NIH award, S10RR025671, for MRI/S instrumentation.

Conflict of interest

The authors declare that the research was conducted in the absence of any commercial or financial relationships that could be construed as a potential conflict of interest.

Generative AI statement

The author(s) declare that no Generative AI was used in the creation of this manuscript.

Supplementary material

The Supplementary Material for this article can be found online at: https://www.frontierspartnerships.org/articles/10.3389/dyst.2025.13874/full#supplementary-material

SUPPLEMENTARY FIGURE S1
Manually drawn brain mask (red region) according to Allen Reference Atlas-Mouse Brain[1]. The mask included relevant dystonia related regions (including cerebellum, vermis, medulla oblongata, pons, midbrain, thalamus, cortex, striatum).

References

1. Bressman SB. Genetics of dystonia: an overview. *Parkinsonism Relat Disord* (2007) 13(Suppl. 3):S347–S355. doi:10.1016/S1353-8020(08)70029-4

2. Ozelius LJ, Hewett JW, Pagel CE, Bressman SB, Kramer PL, Shalish C, et al. The early-onset torsion dystonia gene (DYT1) encodes an ATP-binding protein. *Nat Genet* (1997) 17:40–8. doi:10.1038/ng0997-40

3. Goodchild RE, Dauer WT. Mislocalization to the nuclear envelope: an effect of the dystonia-causing torsinA mutation. *Proc Natl Acad Sci U S A* (2004) 101(3): 847–52. doi:10.1073/pnas.0304375101

4. Granata A, Watson R, Collinson LM, Schiavo G, Warner TT. The dystonia-associated protein TorsinA modulates synaptic vesicle recycling. *J Biol Chem* (2008) 283(12):7568–79. doi:10.1074/jbc.M704097200

5. Chen P, Burdette AJ, Porter JC, Ricketts JC, Fox SA, Nery FC, et al. The early-onset torsion dystonia-associated protein, torsinA, is a homeostatic regulator of endoplasmic reticulum stress response. *Hum Mol Genet* (2010) 19(18):3502–15. doi:10.1093/hmg/ddq266

6. Augood SJ, Keller-McGandy CE, Siriani A, Hewett J, Ramesh V, Sapp E, et al. Distribution and ultrastructural localization of torsinA immunoreactivity in the human brain. *Brain Res* (2003) 986(1–2):12–21. doi:10.1016/s0006-8993(03)03164-0

7. Eskow Jaunarajs KL, Bonsi P, Chesselet MF, Standaert DG, Pisani A. Striatal cholinergic dysfunction as a unifying theme in the pathophysiology of dystonia. *Prog Neurobiol* (2015) 127-128:91–107. doi:10.1016/j.pneurobio.2015.02.002

8. Vitek JL. Pathophysiology of dystonia: a neuronal model. *Movement Disord* (2002) 17:S49–S62. doi:10.1002/mds.10142

9. Prudente CN, Hess EJ, Jinnah HA. Dystonia as a network disorder: what is the role of the cerebellum? *Neuroscience* (2014) 260:23–35. doi:10.1016/j.neuroscience.2013.11.062

10. Shakkottai VG, Batla A, Bhatia K, Dauer WT, Dresel C, Niethammer M, et al. Current opinions and areas of consensus on the role of the cerebellum in dystonia. *Cerebellum* (2017) 16:577–94. doi:10.1007/s12311-016-0825-6

11. Jinnah HA, Neychev V, Hess EJ. The anatomical basis for dystonia: the motor network model. *Tremor and other hyperkinetic movements* (2017) 7:506. doi:10.7916/D8V69X3S

12. Loens S, Verrel J, Herrmann VM, Kienzle A, Tzvi E, Weissbach A, et al. Motor learning deficits in cervical dystonia point to defective basal ganglia circuitry. *Sci Rep* (2021) 11(1):7332. doi:10.1038/s41598-021-86513-7

13. Chen CH, Fremont R, Arteaga-Bracho EE, Khodakhah K. Short latency cerebellar modulation of the basal ganglia. *Nat Neurosci* (2014) 17(12):1767–75. doi:10.1038/nn.3868

14. Kaji R, Bhatia K, Graybiel AM. Pathogenesis of dystonia: is it of cerebellar or basal ganglia origin? *J Neurol Neurosurg Psychiatry NLM (Medline)* (2018) 89: 488–92. doi:10.1136/jnnp-2017-316250

15. Eidelberg D, Moeller JR, Antonini A, Kazumata K, Nakamura T, Dhawan V, et al. Functional brain networks in DYT1 dystonia. *Ann Neurol* (1998) 44(3): 303–12. doi:10.1002/ana.410440304

16. Carbon M, Kingsley PB, Tang C, Bressman S, Eidelberg D. Microstructural white matter changes in primary torsion dystonia. *Movement Disord* (2008) 23(2): 234–9. doi:10.1002/mds.21806

17. Argyelan M, Carbon M, Niethammer M, Uluğ AM, Voss HU, Bressman SB, et al. Cerebellothalamocortical connectivity regulates penetrance in dystonia. *J Neurosci* (2009) 29(31):9740–7. doi:10.1523/JNEUROSCI.2300-09.2009

18. Dang MT, Yokoi F, McNaught KSP, Jengelley TA, Jackson T, Li J, et al. Generation and characterization of Dyt1 DeltaGAG knock-in mouse as a model for early-onset dystonia. *Exp Neurol* (2005) 196(2):452–63. doi:10.1016/j.expneurol.2005.08.025

19. DeAndrade MP, Trongnetrpunya A, Yokoi F, Cheetham CC, Peng N, Wyss JM, et al. Electromyographic evidence in support of a knock-in mouse model of DYT1 Dystonia. *Movement Disord* (2016) 31(11):1633–9. doi:10.1002/mds.26677

20. Uluğ AM, Vo A, Argyelan M, Tanabe L, Schiffer WK, Dewey S, et al. Cerebellothalamocortical pathway abnormalities in torsinA DYT1 knock-in mice. *Proc Natl Acad Sci U S A* (2011) 108(16):6638–43. doi:10.1073/pnas.1016445108

21. Vo A, Sako W, Niethammer M, Carbon M, Bressman SB, Ulug AM, et al. Thalamocortical connectivity correlates with phenotypic variability in dystonia. *Cereb Cortex* (2015) 25(9):3086–94. doi:10.1093/cercor/bhu104

22. Song CH, Bernhard D, Bolarinwa C, Hess EJ, Smith Y, Jinnah HA. Subtle microstructural changes of the striatum in a DYT1 knock-in mouse model of dystonia. *Neurobiol Dis* (2013) 54:362–71. doi:10.1016/j.nbd.2013.01.008

23. Zhang L, Yokoi F, Jin YH, DeAndrade MP, Hashimoto K, Standaert DG, et al. Altered dendritic morphology of Purkinje cells in DYT1 δGAG knock-in and Purkinje cell-specific DYT1 conditional knockout mice. *PLoS One* (2011) 6(3):e18357. doi:10.1371/journal.pone.0018357

24. Pappas SS, Darr K, Holley SM, Cepeda C, Mabrouk OS, Wong JMT, et al. Forebrain deletion of the dystonia protein torsinA causes dystonic-like movements and loss of striatal cholinergic neurons. *Elife* (2015) 4:e08352. doi:10.7554/eLife.08352

25. Yokoi F, Dang MT, Li J, Standaert DG, Li Y. Motor deficits and decreased striatal dopamine receptor 2 binding activity in the striatum-specific Dyt1 conditional knockout mice. *PLoS One* (2011) 6(9):e24539. doi:10.1371/journal.pone.0024539

26. Yokoi F, Dang MT, Mitsui S, Li J, Li Y. Motor deficits and hyperactivity in cerebral cortex-specific Dyt1 conditional knockout mice. *J Biochem* (2008) 143(1):39–47. doi:10.1093/jb/mvm191

27. Wilkes BJ, Adury RZ, Berryman D, Concepcion LR, Liu Y, Yokoi F, et al. Cell-specific Dyt1 ΔGAG knock-in to basal ganglia and cerebellum reveal differential effects on motor behavior and sensorimotor network function. *Exp Neurol* (2023) 367:114471. doi:10.1016/j.expneurol.2023.114471

28. Jin XL, Guo H, Mao C, Atkins N, Wang H, Avasthi PP, et al. Emx1-specific expression of foreign genes using "knock-in" approach. *Biochem Biophys Res Commun* (2000) 270(3):978–82. doi:10.1006/bbrc.2000.2532

29. Weisheit CE, Dauer WT. A novel conditional knock-in approach defines molecular and circuit effects of the DYT1 dystonia mutation. *Hum Mol Genet* (2015) 24(22):6459–72. doi:10.1093/hmg/ddv355

30. Wilkes BJ, DeSimone JC, Liu Y, Chu WT, Coombes SA, Li Y, et al. Cell-specific effects of Dyt1 knock-out on sensory processing, network-level connectivity, and motor deficits. *Exp Neurol* (2021) 343:113783. doi:10.1016/j.expneurol.2021.113783

31. Cox RW. AFNI: Software for analysis and visualization of functional magnetic resonance neuroimages. *Comput Biomed Res* (1996) 29(3):162–73. doi:10.1006/cbmr.1996.0014

32. Avants BB, Yushkevich P, Pluta J, Minkoff D, Korczykowski M, Detre J, et al. The optimal template effect in hippocampus studies of diseased populations. *Neuroimage* (2010) 49(3):2457–66. doi:10.1016/j.neuroimage.2009.09.062

33. Satterthwaite TD, Elliott MA, Gerraty RT, Ruparel K, Loughead J, Calkins ME, et al. An improved framework for confound regression and filtering for control of motion artifact in the preprocessing of resting-state functional connectivity data. *Neuroimage* (2013) 64(1):240–56. doi:10.1016/j.neuroimage.2012.08.052

34. Chu WT, DeSimone JC, Riffe CJ, Liu H, Chakrabarty P, Giasson BI, et al. α-Synuclein induces progressive changes in brain microstructure and sensory-evoked brain function that precedes locomotor decline. *J Neurosci* (2020) 40(34):6649–59. doi:10.1523/JNEUROSCI.0189-20.2020

35. Chen G, Adleman NE, Saad ZS, Leibenluft E, Cox RW. Applications of multivariate modeling to neuroimaging group analysis: a comprehensive alternative to univariate general linear model. *Neuroimage.* (2014) 99:571–88. doi:10.1016/j.neuroimage.2014.06.027

36. Cox RW, Chen G, Glen DR, Reynolds RC, Taylor PA. FMRI clustering and false-positive rates. *Proc Natl Acad Sci USA* (2017) 114:E3370–1. doi:10.1073/pnas.1614961114

37. Tournier JD, Smith R, Raffelt D, Tabbara R, Dhollander T, Pietsch M, et al. MRtrix3: a fast, flexible and open software framework for medical image processing and visualisation. *NeuroImage* (2019) 202:116137. doi:10.1016/j.neuroimage.2019.116137

38. Cordero-Grande L, Christiaens D, Hutter J, Price AN, Hajnal JV. Complex diffusion-weighted image estimation via matrix recovery under general noise models. *Neuroimage* (2019) 200:391–404. doi:10.1016/j.neuroimage.2019.06.039

39. Veraart J, Fieremans E, Novikov DS. Diffusion MRI noise mapping using random matrix theory. *Magn Reson Med* (2016) 76(5):1582–93. doi:10.1002/mrm.26059

40. Kellner E, Dhital B, Kiselev VG, Reisert M. Gibbs-ringing artifact removal based on local subvoxel-shifts. *Magn Reson Med* (2016) 76(5):1574–81. doi:10.1002/mrm.26054

41. Andersson JLR, Sotiropoulos SN. An integrated approach to correction for off-resonance effects and subject movement in diffusion MR imaging. *Neuroimage* (2016) 125:1063–78. doi:10.1016/j.neuroimage.2015.10.019

42. Andersson JLR, Skare S, Ashburner J. How to correct susceptibility distortions in spin-echo echo-planar images: application to diffusion tensor imaging. *Neuroimage* (2003) 20(2):870–88. doi:10.1016/S1053-8119(03)00336-7

43. Smith SM, Jenkinson M, Woolrich MW, Beckmann CF, Behrens TEJ, Johansen-Berg H, et al. Advances in functional and structural MR image analysis and implementation as FSL. *NeuroImage.* (2004) 23:S208–S219. doi:10.1016/j.neuroimage.2004.07.051

44. Hoy AR, Koay CG, Kecskemeti SR, Alexander AL. Optimization of a free water elimination two-compartment model for diffusion tensor imaging. *Neuroimage* (2014) 103:323–33. doi:10.1016/j.neuroimage.2014.09.053

45. Pasternak O, Sochen N, Gur Y, Intrator N, Assaf Y. Free water elimination and mapping from diffusion MRI. *Magn Reson Med* (2009) 62(3):717–30. doi:10.1002/mrm.22055

46. Neto Henriques R, Rokem A, Garyfallidis E, St-Jean S, Peterson ET, Correia MM. [Re] Optimization of a free water elimination two-compartment model for diffusion tensor imaging. *Cold Spring Harbor Lab* (2017). doi:10.1101/108795

47. Avanzino L, Abbruzzese G. How does the cerebellum contribute to the pathophysiology of dystonia? *Basal Ganglia* (2012) 2(4):231–5. doi:10.1016/j.baga.2012.05.003

48. Desrochers P, Brunfeldt A, Sidiropoulos C, Kagerer F. Sensorimotor control in dystonia. *Brain Sci* (2019) 9:79. doi:10.3390/brainsci9040079

49. Vo A, Nguyen N, Fujita K, Schindlbeck KA, Rommal A, Bressman SB, et al. Disordered network structure and function in dystonia: pathological connectivity vs. adaptive responses. *Cereb Cortex* (2023) 33(11):6943–58. doi:10.1093/cercor/bhad012

50. Popa LS, Ebner TJ. Cerebellum, predictions and errors. *Front Cell Neurosci* (2019) 12:524. doi:10.3389/fncel.2018.00524

51. Meoni S, Macerollo A, Moro E. Sex differences in movement disorders. *Nat Rev Neurol* (2020) 16:84–96. doi:10.1038/s41582-019-0294-x

52. Gilio F, Currà A, Inghilleri M, Lorenzano C, Suppa A, Manfredi M, et al. Abnormalities of motor cortex excitability preceding movement in patients with dystonia. *Brain* (2003) 126(8):1745–54. doi:10.1093/brain/awg188

53. Carbon M, Argyelan M, Ghilardi MF, Mattis P, Dhawan V, Bressman S, et al. Impaired sequence learning in dystonia mutation carriers: a genotypic effect. *Brain* (2011) 134(5):1416–27. doi:10.1093/brain/awr060

54. Liang CC, Tanabe LM, Jou S, Chi F, Dauer WT. TorsinA hypofunction causes abnormal twisting movements and sensorimotor circuit neurodegeneration. *J Clin Invest* (2014) 124(7):3080–92. doi:10.1172/JCI72830

55. DeSimone JC, Febo M, Shukla P, Ofori E, Colon-Perez LM, Li Y, et al. *In vivo* imaging reveals impaired connectivity across cortical and subcortical networks in a mouse model of DYT1 dystonia. *Neurobiol Dis* (2016) 95:35–45. doi:10.1016/j.nbd.2016.07.005

56. Dang MT, Yokoi F, Cheetham CC, Lu J, Vo V, Lovinger DM, et al. An anticholinergic reverses motor control and corticostriatal LTD deficits in Dyt1 ΔGAG knock-in mice. *Behav Brain Res* (2012) 226(2):465–72. doi:10.1016/j.bbr.2011.10.002

57. Liu Y, Xing H, Yokoi F, Vaillancourt DE, Li Y. Investigating the role of striatal dopamine receptor 2 in motor coordination and balance: insights into the pathogenesis of DYT1 dystonia. *Behav Brain Res* (2021) 403. doi:10.1016/j.bbr.2021.113137

58. Vo A, Eidelberg D, Uluğ AM. White matter changes in primary dystonia determined by 2D distribution analysis of diffusion tensor images. *J Magn Reson Imaging* (2013) 37(1):59–66. doi:10.1002/jmri.23805

59. Carbon M, Kingsley PB, Su S, Smith GS, Spetsieris P, Bressman S, et al. Microstructural white matter changes in carriers of the DYT1 gene mutation. *Ann Neurol* (2004) 56(2):283–6. doi:10.1002/ana.20177

60. DeSimone JC, Pappas SS, Febo M, Burciu RG, Shukla P, Colon-Perez LM, et al. Forebrain knock-out of torsinA reduces striatal free-water and impairs whole-brain functional connectivity in a symptomatic mouse model of DYT1 dystonia. *Neurobiol Dis* (2017) 106:124–32. doi:10.1016/j.nbd.2017.06.015

61. Vo A, Sako W, Dewey SL, Eidelberg D, Uluğ AM. 18FDG-microPET and MR DTI findings in Tor1a+/- heterozygous knock-out mice. *Neurobiol Dis* (2015) 73: 399–406. doi:10.1016/j.nbd.2014.10.020

62. Song CH, Fan X, Exeter CJ, Hess EJ, Jinnah HA. Functional analysis of dopaminergic systems in a DYT1 knock-in mouse model of dystonia. *Neurobiol Dis* (2012) 48(1):66–78. doi:10.1016/j.nbd.2012.05.009

63. Hewett J, Johanson P, Sharma N, Standaert D, Balcioglu A. Function of dopamine transporter is compromised in DYT1 transgenic animal model *in vivo*. *J Neurochem* (2010) 113(1):228–35. doi:10.1111/j.1471-4159.2010.06590.x

64. Horisawa S, Arai T, Suzuki N, Kawamata T, Taira T. The striking effects of deep cerebellar stimulation on generalized fixed dystonia: case report. *J Neurosurg* (2020) 132(3):712–6. doi:10.3171/2018.11.JNS182180

65. Horisawa S, Kohara K, Nonaka T, Mochizuki T, Kawamata T, Taira T. Case report: deep cerebellar stimulation for tremor and dystonia. *Front Neurol* (2021) 12: 642904. doi:10.3389/fneur.2021.642904

66. Brown EG, Bledsoe IO, Luthra NS, Miocinovic S, Starr PA, Ostrem JL. Cerebellar deep brain stimulation for acquired hemidystonia. *Mov Disord Clin Pract* (2020) 7(2):188–93. doi:10.1002/mdc3.12876

67. Romito LM, Franzini A, Perani D, Carella F, Marras C, Capus L, et al. Fixed dystonia unresponsive to pallidal stimulation improved by motor cortex stimulation. *Neurology* (2007) 68(11):875–6. doi:10.1212/01.wnl.0000256816.83036.c9